Journal of Materials Chemistry A

PAPER

View Article Online
View Journal | View Issue

Cite this: J. Mater. Chem. A, 2016, 4, 6070

Ultrasensitive reversible oxygen sensing by using liquid-exfoliated MoS_2 nanoparticles†

Yeon Hoo Kim,‡[a] Kye Yeop Kim,‡[a] You Rim Choi,[a] Young-Seok Shim,[a] Jong-Myeong Jeon,[a] Jong-Heun Lee,[b] Soo Young Kim,[c] Seungwu Han*[a] and Ho Won Jang*[a]

Received 11th February 2016
Accepted 20th March 2016

DOI: 10.1039/c6ta01277a

www.rsc.org/MaterialsA

Two-dimensional (2D) molybdenum disulfide (MoS_2) has been attracting rapidly increasing interest for application in chemoresistive gas sensors owing to its moderate band gap energy and high specific surface area. However, the mechanism of chemoresistive sensing *via* the adsorption and desorption of gas molecules and the influence of the shape of 2D materials are not well understood yet. Herein we investigate the oxygen sensing behavior of MoS_2 microflakes and nanoparticles prepared by mechanical and liquid exfoliation, respectively. Liquid-exfoliated MoS_2 nanoparticles with an increased number of edge sites present high and linear responses to a broad range of oxygen concentrations (1–100%). The energetically favorable oxygen adsorption sites, which are responsible for reversible oxygen sensing, are identified by first-principles calculations based on density functional theory. This study serves as a proof-of-concept for the gas sensing mechanism depending on the surface configuration of 2D materials and broadens the potential of 2D MoS_2 in gas sensing applications.

Introduction

In modern society, managing air quality is essential for enhancing the quality of human life. The high concentrations of fine dust, CO, NO_2, SO_2 and CO_2 cause complex respiratory diseases and hamper the productivity and learning ability in work places.[1] Furthermore, as the Internet of Things (IoT), interconnected devices capable of exchanging their own information about the internal state and the external environment with users or other devices, attracts attention, monitoring air quality becomes a requisite function for next-generation electronics.[2]

Until now, the concentrations of CO, NO_2, SO_2, and CO_2 have been measured at the parts-per-million (ppm) level for monitoring air quality, because exposure to small portions of these gases can have a detrimental effect on human health. Detecting the oxygen concentration in percentage terms is also important because low levels of oxygen can produce negative symptoms in humans. The symptoms of increased heart and breathing rates and impaired attention are caused by oxygen concentrations >16%. In a harsh environment, workers can become asphyxiated at oxygen concentrations below 12% (Table S1†).[3] Moreover, the oxygen concentration should be maintained at a certain level for particular applications like incubators for premature infants, and cell culture media. The development of oxygen gas sensors that can detect oxygen over a broad concentration range is desired for varied applications.

Chemoresistive gas sensors based on semiconducting materials are considered promising candidates for emerging applications such as IoT and flexible electronics due to their facile fabrication processes, small sizes, low costs, and easy integration into integrated circuits. However, commercialized oxygen sensors are mostly based on electrochemical gas sensors. These sensors have complex structures and hardly provide high reliability and linearity over a wide range of oxygen concentrations, which limit their applicability in IoT and flexible electronics.[4]

2D materials are gaining increasing attention in this field as prospective sensing materials because surfaces without bulk offer high surface-to-volume ratios, and surface configurations including dangling bonds on the edge sites and basal planes can be easily modified. Moreover, facile surface modification with charge-transfer doping effects readily improves the gas sensing properties.[5–7] In particular, MoS_2, a layered semiconducting transition metal dichalcogenide, has shown interesting gas sensing properties owing to its high surface-to-volume ratio, semiconducting nature, and numerous active edge sites.[8–13] However, despite the increasing attention and the

[a]Department of Materials Science and Engineering, Research Institute for Advanced Materials, Seoul National University, Seoul 08826, Republic of Korea. E-mail: hwjang@snu.ac.kr; hansw@snu.ac.kr

[b]Department of Materials Science and Engineering, Korea University, Seoul 136-713, Republic of Korea

[c]School of Chemical Engineering and Materials Science, Chung-Ang University, Seoul 06974, Republic of Korea

† Electronic supplementary information (ESI) available. See DOI: 10.1039/c6ta01277a

‡ These authors contributed equally to this work.

diverse research studies, studies on the relationship between the gas sensing mechanism and the edge sites of 2D MoS_2 have not been achieved yet.

Herein, we report the comparative oxygen sensing behaviours of liquid-exfoliated MoS_2 nanoparticles and mechanically exfoliated MoS_2 microflakes. The sensors prepared by drop-casting methods on Pt interdigitated electrodes (IDEs) exhibit a high and linear response to a wide range of oxygen concentrations due to the increased number of active edge sites. The adsorbed oxygen promotes the interaction kinetics between the reducing gases and the sensing materials, resulting in high sensitivity to ethanol at a parts-per-billion (ppb) level under ambient conditions.[14–20] First-principles calculations were conducted to estimate the oxygen adsorption energies based on the surface configuration of the 2D materials. The calculations reveal the critical role played by the specific adsorption sites in the reversible and high oxygen response.

Experimental section

Materials

The procedures for exfoliating MoS_2 into nanoparticles were adapted from a previous report and slightly modified.[21] Briefly, natural molybdenum sulfide powder (MoS_2, Sigma-Aldrich) was immersed into *N*,*N*-dimethylformamide (DMF, Sigma-Aldrich) at an initial concentration of 10 mg mL^{-1} followed by ultrasonication at 60 Hz for 12 hours. The mixture was washed by centrifugation at 14 000 rpm for 15 minutes 4 times, changing DMF into distilled water. The obtained solution was centrifuged at 2000 rpm for 30 minutes, and the top 2/3 of the supernatant was collected. The precipitated solid was re-dispersed in distilled water at a concentration of ~2 mg mL^{-1}.

Sensor fabrication

IDEs of 4 μm interspacing were prepared on a SiO_2/Si substrate using photolithography followed by metal (Pt/Ti) deposition by e-beam evaporation. A 2 μg drop of 2 mg mL^{-1} MoS_2 nanoparticle solution was cast onto a Pt IDE/SiO_2/Si substrate and was then dried for 30 minutes at 100 °C. The fabricated sensors were annealed at 300 °C for 20 minutes. To prepare SnO_2 nanosphere sensors, an aqueous suspension of 300 nm-diameter polystyrene (PS) beads was used. The PS beads were spin-coated on an O_2 plasma treated Pt IDE/SiO_2/Si substrate. A 70 nm-thick SnO_2 film was deposited onto the PS template by room-temperature radio frequency sputtering. The sample was calcined in air at 500 °C for 1 hour to burn out the polymer beads and simultaneously crystallize the SnO_2 film, resulting in a nanosphere film on the substrate.

Characterization

MoS_2 nanoparticles on a Si substrate were characterized by using a scanning electron microscope (FE-SEM, MERLIN Compact, ZEISS) using 1 kV. For the TEM study, MoS_2 nanoparticles were deposited on quantifoil Cu grids (300 mesh holey carbon). The TEM experiments were performed by using a JEM-2100F. The AFM image (NANO Station II, Surface Imaging system) was obtained in the non-contact mode. Raman scattering was performed on a Raman spectrometer with excitation by 640 nm laser light. XPS was carried out at 4D beamlines at Pohang Accelerator Laboratory (PAL).

Sensor measurements

The gas sensing properties of the fabricated MoS_2 nanoparticle sensor and the SnO_2 nanosphere sensor were measured at 300 °C by monitoring the variation in sensor resistance on changing the flow gas from dry air to a calibrated test gas (balanced with dry air). The sensor resistance was measured under a DC bias voltage of 3 V using a source measurement unit (Keithley 236). A constant flow rate of 500 sccm was used for dry air and the test gases. The response of the sensors was accurately determined by the ratio of the fully saturated resistances after exposure to the test gases to the base resistances in dry air.

Calculations

All first-principles calculations in this study were performed using the Vienna *ab Initio* simulation package (VASP).[22] The electron–ion interaction is described by projected-augmented wave (PAW) pseudopotential.[23] We employ PBE for exchange-correlation functional.[24] A plane-wave cutoff of 350 eV and a 40 × 1 × 1 *k*-point grid were used for the unit cell of a semi-infinite stripe of MoS_2. All the atomic coordinates were relaxed within 0.03 eV $Å^{-1}$. For modeling edge sites, a semi-infinite stripe of MoS_2 ribbon having a width of 6 Mo atoms was used. To investigate how the width of MoS_2 flakes affects the simulation, the density of states of each layer for MoS_2 flakes with widths of 12 unit cells and 6 unit cells, and a bulk MoS_2 layer of infinite unit cells was investigated (Fig. S1†). The effect of O_2 coverage on G_{ad} was studied by multiplying the periodicity of O_2 adsorption given in Fig. 3 by two or four times but G_{ad} changes within 0.01 eV.

Results and discussion

For comparative analysis of the gas sensors prepared by different exfoliation methods, two types of MoS_2 gas sensors were fabricated by mechanical and liquid exfoliation methods from the same MoS_2 single crystal (Fig. 1a). Over the entire fabrication process, any chemicals which could modify the chemical sensing properties of MoS_2 were not added. Fig. 1b and c show the scanning electron microscopy (SEM) and atomic force microscopy (AFM) images of the mechanically exfoliated MoS_2 microflakes and Fig. 1d and e show the images of the liquid-exfoliated MoS_2 nanoparticles deposited between the Pt IDEs. The mechanically exfoliated MoS_2 sensor was prepared by the scotch tape method,[25] in which the MoS_2 microflakes with an average size of 5 μm were sparsely attached to the substrate (Fig. S2†). On the other hand, the liquid-exfoliated MoS_2 nanoparticles were deposited on the Pt IDEs by the drop-casting method and the nanoparticles were uniformly distributed with smaller sizes (~100 nm wide and ~15 nm high). These particle shapes imply a higher ratio of edge sites for the liquid-exfoliated MoS_2 nanoparticles. Raman scattering was performed on

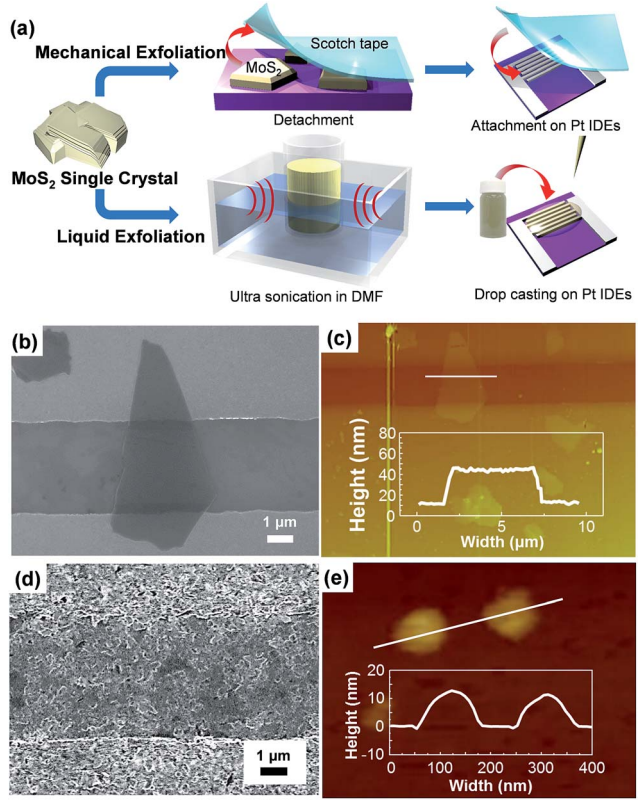

Fig. 1 (a) Fabrication procedure of mechanically and liquid-exfoliated MoS_2 gas sensors. SEM and AFM images of (b and c) mechanically exfoliated MoS_2 microflakes and (d and e) liquid-exfoliated MoS_2 nanoparticles deposited between Pt IDEs.

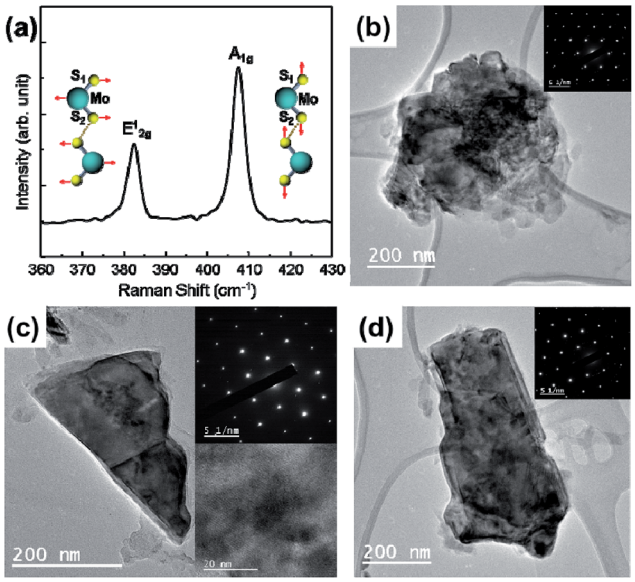

Fig. 2 (a) Raman spectrum of liquid-exfoliated MoS_2. (b–d) TEM images of liquid-exfoliated MoS_2 nanoparticles with different shapes. Upper insets show the corresponding electron diffraction pattern and the lower inset in (c) is a HRTEM image of the MoS_2 single crystal.

a Raman spectrometer with excitation by 640 nm laser light. Fig. 2a shows the Raman spectrum of the liquid-exfoliated MoS_2 nanoparticles, which reveals the in-plane vibrational modes of the Mo and S atoms (E^1_{2g}) and the out-of-plane vibrational mode of the S atoms (A_{1g}).[26,27] Transmission electron microscopy (TEM) images were taken from different liquid-exfoliated MoS_2 nanoparticles (Fig. 2b–d). The upper inset in each TEM image shows the corresponding electron diffraction pattern and the lower inset in Fig. 1c is a high-resolution transmission electron microscopy (HRTEM) image of the liquid-exfoliated MoS_2 nanoparticles. The electron diffraction pattern obtained from the liquid-exfoliated MoS_2 nanoparticles reveals their single-crystalline nature. X-ray photoemission spectroscopy (XPS) was performed on the as-deposited MoS_2 nanoparticles and the particles after heat treatment at 300 °C under ambient conditions (21% O_2 and 79% N_2). A MoO_3 peak is observed after the heat treatment, which demonstrates the adsorption of oxygen on MoS_2 surfaces (Fig. S3†).

The response curves of the mechanically and liquid-exfoliated MoS_2 sensors were measured for O_2 concentrations up to 100% at elevated temperatures of 200, 300, and 400 °C (Fig. 3a and b). The responses of the sensors were accurately determined by the ratio of the fully saturated resistances after exposure to the test gas (O_2) to the base resistances in nitrogen (N_2). The response is defined as R_{O_2}/R_{N_2} for the reducing gases where R_{O_2} and R_{N_2} denote resistances of the sensor in O_2 and in N_2, respectively. For the mechanically exfoliated MoS_2 sensor, the response to O_2 increased with increasing temperature but the response is as low as 1.5 at 400 °C and the sensor shows irreversible and retarded gas sensing behaviours. In addition, the sensor exhibits a high electrical noise level with unstable base resistance. In contrast, the liquid-exfoliated MoS_2 sensor shows a response as high as ~5700 at 400 °C. The liquid-exfoliated MoS_2 sensor exhibits higher responses to O_2 at all the elevated temperatures (Fig. 3c). The sensors show huge differences in sensing properties according to their fabrication methods. It may be attributed to the modified surface-to-volume ratio and the consequent change in the number of edge sites. Additional measurements were performed at 300 °C because the base resistance is unstable at the elevated temperature of 400 °C. Fig. 4a shows a dynamic sensing transient of the liquid-exfoliated MoS_2 sensor to four consecutive pulses of 100% O_2 at 300 °C. The device shows high stability and full recovery to the four pulses of O_2 without shifting the base resistance or responses. The responses of the sensor to 2–100% of O_2 at 300 °C as shown in Fig. 4b were measured. The responses of the liquid-exfoliated MoS_2 sensor were 8.69, 10.83, 12.25, 13.73, 17.4, 23.98, 29.96, 50.28, and 63.73 to 2, 5, 7, 10, 15, 25, 50, 75, and 100% O_2, respectively. The linear relationship between the response and O_2 gas concentration indicates that the operational capabilities of the sensor are reliable over a wide concentration range up to 100%. The slope of the plotted line, calculated to be 5453.6 ppm^{-1}, represents the sensitivity of the sensor (Fig. 4c). The plotted line does not seem to meet the zero point when the O_2 concentration goes to zero. However, the response will finally reach the zero point because the response–concentration curve will not be in a linear relationship for very

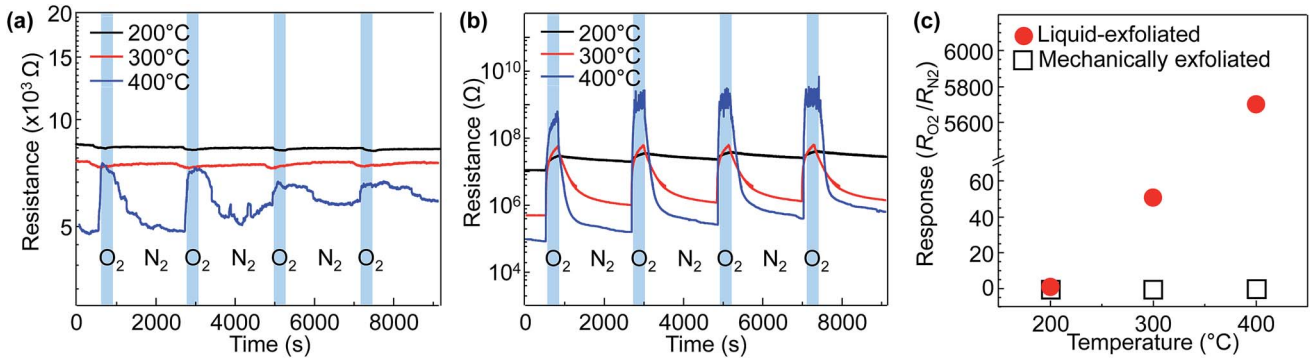

Fig. 3 Response curves of (a) mechanically exfoliated and (b) liquid-exfoliated MoS_2 gas sensors to 100% O_2 at 200, 300, and 400 °C. (c) Responses of mechanically and liquid-exfoliated MoS_2 gas sensors to 100% O_2 as a function of temperature.

low oxygen concentrations such as ppm levels.[28] This extremely high sensitivity and linearity to O_2 concentrations are great merits of 2D MoS_2 with an increased number of edge sites. As far as we are aware, oxygen gas sensors with these outstanding sensing characteristics have never been achieved before this by the chemoresistive method (Table S2†).

The experimental results suggest that the surface configurations of MoS_2 particles prepared by using different exfoliation techniques are critical for gas-sensing properties, *i.e.*, edge sites attract more O_2 molecules than clean surfaces. To confirm this, the adsorption energies of O_2 on MoS_2 were investigated using first-principles calculations based on density functional theory (see Calculations).

First, we calculated the adsorption free energy (G_{ad}) of the O_2 molecule on a clean surface at temperature T and partial pressure P as follows:

$$G_{ad}(T,P) = G(MoS_2 + O_2) - G(MoS_2) - \mu_{O_2}(T,P) \quad (1)$$

where $G(MoS_2 + O_2)$ and $G(MoS_2)$ indicate the free energies of the MoS_2 surface with an O_2 molecule adsorbed on clean MoS_2, respectively, and $\mu_{O_2}(T,P)$ is the gas-phase chemical potential of the O_2 molecule. The experimental conditions are considered in $\mu_{O_2}(T,P)$ as follows:

$$\mu_{O_2}(T,P) = \mu_{O_2}(T,P^0) + k_B T \ln\left(\frac{P}{P^0}\right), \quad (2)$$

where P^0 is 1 atm. In addition,

$$\mu_{O_2}(T,P^0) = \Delta H + T\Delta S\mu_{O_2}(T,P^0) + \mu_{O_2}(0\ K,P^0) \quad (3)$$

where ΔH and ΔS correspond to the enthalpy and entropy changes per molecule between T and 0 K at the standard pressure, respectively, and are obtained from thermodynamical tables.[29] In eqn (3), $\mu_{O_2}(0\ K,P^0)$ is equal to the total energy of the O_2 molecule. Because of the well-known overbinding of the O_2 molecule in density functional theory, we determined this value using the experimental binding energy of 5.23 eV.[30]

For the clean MoS_2 surface, the O_2 molecule was locally stable only at the top of S atoms. However, G_{ad} (300 °C, 1 atm) on this site is 1.72–3.21 eV, meaning that the O_2 molecule would not bind to the clean MoS_2 surface (Fig. S4 and Table S3†). Next, we investigated the energetics of O_2 adsorption on a semi-infinite stripe model of MoS_2. For the termination of the MoS_2 edge, we considered clean Mo-edges (Fig. 5a–c) and Mo-edges with S monomers (Fig. 5d and e). We exclude the S-edge model because the O_2 adsorption is locally unstable. The stable sites of O_2 adsorption on each MoS_2 edge are displayed in Fig. 5a–e with respective G_{ad} (300 °C, 1 atm) values shown under each figure.

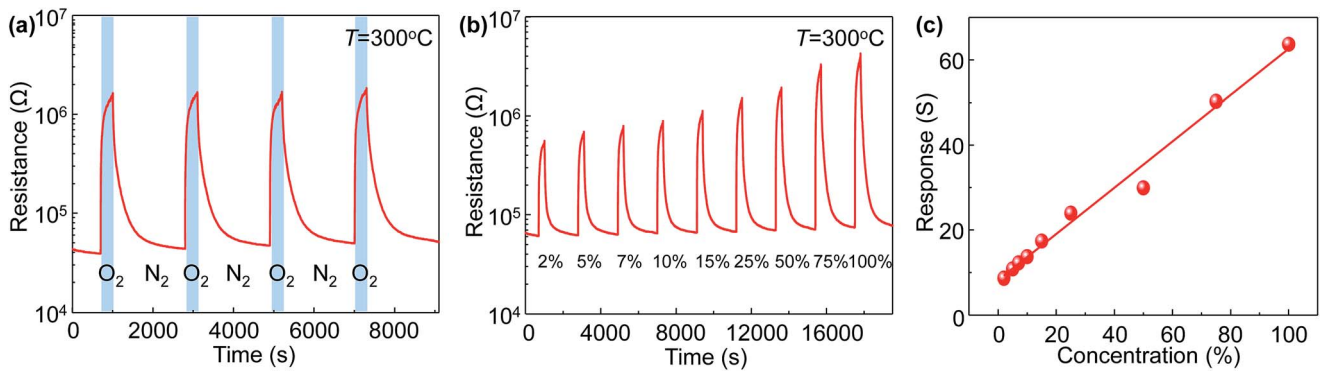

Fig. 4 (a) Response curves of the liquid-exfoliated MoS_2 gas sensor to four pulses of 100% of O_2 at 300 °C. (b) Response curves to different O_2 concentrations at 300 °C. (c) Linear fit of the responses as a function of O_2 at 300 °C.

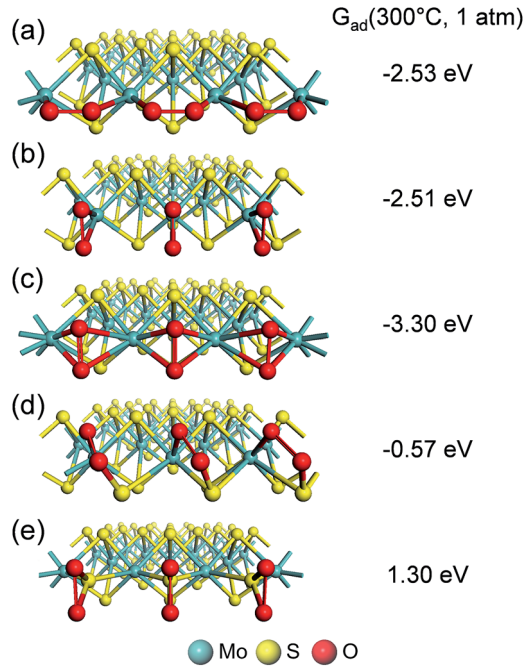

Fig. 5 Stable sites of O_2 adsorption. (a–c) Locally stable configurations of O_2 adsorbed on clean Mo-edges. (d and e) O_2 adsorption on Mo-edges with S monomers. The adsorption free energy at 300 °C and 1 atm [G_{ad} (300 °C, 1 atm)] is displayed.

The G_{ad} values for Mo-edges (−3.30 to −2.51 eV) are much lower than those for Mo-edges with S monomers (−0.57 to 1.30 eV) due to the strong affinity of oxygen to Mo.

To consider the experimental conditions more explicitly, we investigated the effect of oxygen partial pressure on G_{ad} values at each temperature. Fig. 6a and b show the G_{ad} values of O_2 molecules on the Mo–S bridges (Fig. 5d) and the S monomers (Fig. 5e) of Mo-edges with S monomers, respectively. In Fig. 6a, the G_{ad} of O_2 molecules on the Mo–S bridges increases with decreasing P, crossing the zero point at low pressure. This indicates that O_2 desorbs from the Mo–S bridge sites. At lower temperatures of 200 and 300 °C, the crossing of the zero point occurs at much lower partial pressures. This is in qualitative agreement with the above experiment, in which the sensitivity of O_2 sensing improves at high temperatures. On the other hand, Fig. 6b indicates that O_2 does not bind on the S monomers of Mo-edges with S monomers. The G_{ad} values of O_2 molecules on Mo-edges (not shown) confirm that O_2 binds at these edges too strongly to show reversible adsorption/desorption. Therefore, it is clear that only the Mo–S bridges in Fig. 5d allow for reversible O_2 adsorption/desorption among the considered binding sites. We have also investigated the dependence of O_2 adsorption energies for Mo–S bridge sites on O_2 coverage to explain the linear relationship at high oxygen concentrations (Fig. S5†).

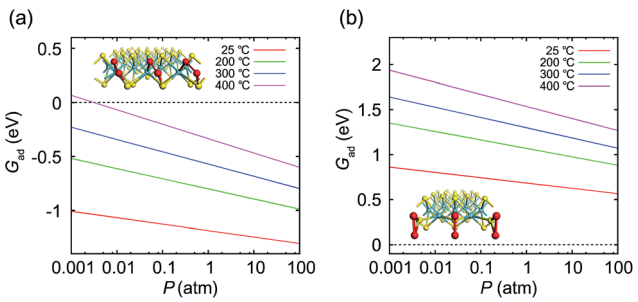

Fig. 6 Adsorption energy of O_2 molecules on (a) Mo–S bridge sites of Mo-edges with S monomers and (b) S monomers of Mo-edges with S monomers with respect to temperature and oxygen partial pressure.

To understand how O_2 adsorption influences the conductivity of a MoS_2 film, we examined the electronic structure of the clean Mo-edges with S monomers both with and without O_2 adsorption. Fig. 7a and b show the band structure (left) and density of states projected on the edge atoms (right) for each model, respectively. The charge distribution near the Fermi level is shown in the bottom figures. In the band structure of the clean Mo–S bridges, the energy band crosses the Fermi level, indicating the metallic character. The colour intensity of the crossing band indicates that the metallic states are localized along the edges. The charge density distribution in the bottom figure shows that the metallic states originate mainly from the d orbitals of Mo atoms on the edges. This was also reported in previous theoretical studies.[31] On the other hand, with O_2 adsorption on the Mo–S bridge sites, the electronic structure undergoes substantial changes (Fig. 7b). The metallic band in Fig. 7a is significantly flattened, meaning that the effective electron mass becomes much higher than that for the clean edges. The large effective electron mass would directly lower the electrical conductivity according to the semiclassical Drude model. The charge distribution at the bottom of Fig. 7b also shows that the electronic states are more localized along the edges in comparison with Fig. 7a.

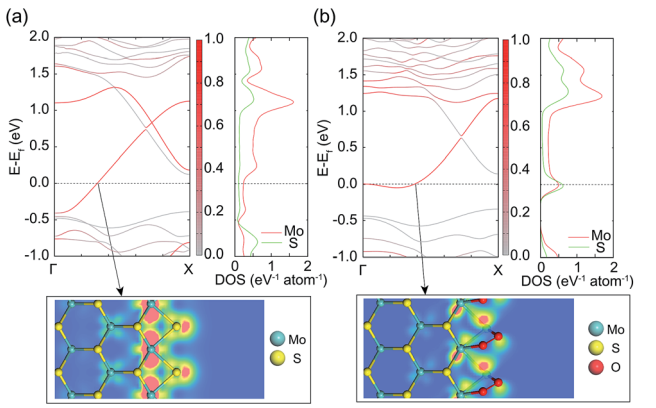

Fig. 7 Band structure, density of states (DOS) of edge atoms and charge density distribution near the Fermi level of (a) clean Mo-edges with S monomers and (b) O_2 adsorbed Mo-edges with S monomers on the Mo–S bridge site. The color intensity in the band structure is proportional to the weight of the corresponding state on the edge atoms; red and gray mean edge atoms and the other atoms, respectively. Red and blue in charge density distribution indicate the maximum and zero electronic densities, respectively.

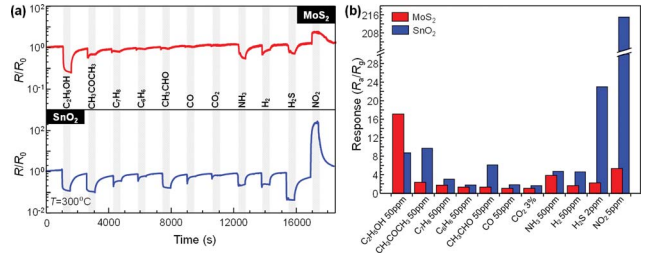

Fig. 8 (a) Sensing transients of liquid-exfoliated MoS_2 and SnO_2 nanosphere gas sensors to various gases. (b) Response of liquid-exfoliated MoS_2 nanoparticle and SnO_2 nanosphere gas sensors to various gases.

Fig. 8a shows dynamic sensing transients of the liquid-exfoliated MoS_2 sensor and SnO_2 nanosphere sensor to 50 ppm of C_2H_5OH, CH_3COCH_3, C_7H_8, C_6H_6, CH_3CHO, CO, NH_3, and H_2, 3% of CO_2, 2 ppm of H_2S, and 5 ppm of NO_2 at 300 °C. The SnO_2 sensor was fabricated using sputtering, the experimental details of which are mentioned in our previous report.[32] Their responses are shown in Fig. 8b. In previous studies, it has been demonstrated that pre-adsorbed O_2 molecules on semiconducting metal oxides play a major role in the sensing reaction to reducing gases.[14–20] Similarly, the liquid-exfoliated MoS_2 sensor exhibits high selectivity for C_2H_5OH because of a large number of pre-adsorbed O_2 molecules on the MoS_2. On the other hand, the response of the liquid-exfoliated MoS_2 sensor to NO_2, 5, is lower than that of the SnO_2 sensor, 215. Direct adsorption is proposed for NO_2 without any interaction with pre-adsorbed molecules ($NO_2 + e^- \rightarrow NO_2^-$).[33] Since the liquid-exfoliated MoS_2 exhibits extremely high oxygen sensitivity, most adsorption sites may have been occupied with pre-adsorbed O_2 molecules. Accordingly, no unoccupied adsorption sites were left for NO_2. Thus, the liquid-exfoliated MoS_2 sensor has comparatively higher selectivity to C_2H_5OH and a lower response to NO_2 than the SnO_2 sensor. Furthermore, to evaluate the detection limit for C_2H_5OH, the response of the MoS_2 sensor was measured over the 3–50 ppm concentration range. The minimum detection limit of the proposed sensor for C_2H_5OH is determined to be 49.96 ppb at 300 °C (Fig. S6†).[34,35]

Conclusions

In conclusion, we have reported the high oxygen sensitivity of a liquid-exfoliated MoS_2 gas sensor prepared by facile fabrication steps. The liquid-exfoliated MoS_2 gas sensor demonstrates high responses with wide concentration range stability to O_2. The high response of liquid-exfoliated MoS_2 nanoparticles to O_2 molecules is attributed to the semiconducting nature of MoS_2 and the increased number of edge sites developed by liquid exfoliation. First-principles calculations revealed the critical role of the edge sites, which can be easily modified by fabrication procedures, in O_2 sensing. We believe that the outstanding device performance demonstrated in this study has proven the potential of MoS_2-based oxygen gas sensors in practical applications.

Acknowledgements

This study was financially supported by the Center for Integrated Smart Sensors funded by the Ministry of Science, ICT & Future Planning as the Global Frontier Project, the Outstanding Young Researcher Program, and the Fusion Research Program for Green Technologies through the National Research Foundation of Korea.

Notes and references

1 J. D. Spengler and K. Sexton, *Science*, 1983, **221**, 9–17.
2 D. Miorandi, S. Sicari, F. De Pellegrini and I. Chlamtac, *Ad Hoc Networks*, 2012, **10**, 1497–1516.
3 N. McManus, *Safety and health in confined spaces*, CRC Press, 1998.
4 T. Takeuchi, *Sens. Actuators, B*, 1988, **14**, 109–124.
5 W. Xu, T. S. Lim, H. K. Seo, S. Y. Min, H. Cho, M. H. Park, Y. H. Kim and T. W. Lee, *Small*, 2014, **10**, 1999–2005.
6 W. Xu, H. K. Seo, S. Y. Min, H. Cho, T. S. Lim, C. y. Oh, Y. Lee and T. W. Lee, *Adv. Mater.*, 2014, **26**, 3459–3464.
7 W. Xu, L. Wang, Y. Liu, S. Thomas, H. K. Seo, K. I. Kim, K. S. Kim and T. W. Lee, *Adv. Mater.*, 2015, **27**, 1619–1623.
8 B. Cho, M. G. Hahm, M. Choi, J. Yoon, A. R. Kim, Y.-J. Lee, S.-G. Park, J.-D. Kwon, C. S. Kim and M. Song, *Sci. Rep.*, 2015, **5**, 8052.
9 Q. He, Z. Zeng, Z. Yin, H. Li, S. Wu, X. Huang and H. Zhang, *Small*, 2012, **8**, 2994–2999.
10 D. J. Late, Y.-K. Huang, B. Liu, J. Acharya, S. N. Shirodkar, J. Luo, A. Yan, D. Charles, U. V. Waghmare and V. P. Dravid, *ACS Nano*, 2013, **7**, 4879–4891.
11 H. Li, Z. Yin, Q. He, H. Li, X. Huang, G. Lu, D. W. H. Fam, A. I. Y. Tok, Q. Zhang and H. Zhang, *Small*, 2012, **8**, 63–67.
12 B. Liu, L. Chen, G. Liu, A. N. Abbas, M. Fathi and C. Zhou, *ACS Nano*, 2014, **8**, 5304–5314.
13 F. K. Perkins, A. L. Friedman, E. Cobas, P. Campbell, G. Jernigan and B. T. Jonker, *Nano Lett.*, 2013, **13**, 668–673.
14 Y. Chen, X. Xue, Y. Wang and T. Wang, *Appl. Phys. Lett.*, 2005, **87**, 233503.
15 T. Gao and T. Wang, *Appl. Phys. A: Mater. Sci. Process.*, 2005, **80**, 1451–1454.
16 T.-J. Hsueh, C.-L. Hsu, S.-J. Chang and I.-C. Chen, *Sens. Actuators, B*, 2007, **126**, 473–477.
17 Y. Liang, Y. Chen and T. Wang, *Appl. Phys. Lett.*, 2004, **85**, 666–668.
18 R. W. Scott, S. Yang, G. Chabanis, N. Coombs, D. Williams and G. Ozin, *Adv. Mater.*, 2001, **13**, 1468–1472.
19 Y. Shimizu and M. Egashira, *MRS Bull.*, 1999, **24**, 18–24.
20 Q. Wan, Q. Li, Y. Chen, T.-H. Wang, X. He, J. Li and C. Lin, *Appl. Phys. Lett.*, 2004, **84**, 3654–3656.
21 J. N. Coleman, M. Lotya, A. O'Neill, S. D. Bergin, P. J. King, U. Khan, K. Young, A. Gaucher, S. De and R. J. Smith, *Science*, 2011, **331**, 568–571.
22 G. Kresse and J. Hafner, *Phys. Rev. B: Condens. Matter Mater. Phys.*, 1993, **47**, 558.
23 P. E. Blöchl, *Phys. Rev. B: Condens. Matter Mater. Phys.*, 1994, **50**, 17953.

24 J. P. Perdew, K. Burke and M. Ernzerhof, *Phys. Rev. Lett.*, 1996, **77**, 3865.
25 K. Novoselov, D. Jiang, F. Schedin, T. Booth, V. Khotkevich, S. Morozov and A. Geim, *Proc. Natl. Acad. Sci. U. S. A.*, 2005, **102**, 10451–10453.
26 C. Lee, H. Yan, L. E. Brus, T. F. Heinz, J. Hone and S. Ryu, *ACS Nano*, 2010, **4**, 2695–2700.
27 S. J. Sandoval, D. Yang, R. Frindt and J. Irwin, *Phys. Rev. B: Condens. Matter Mater. Phys.*, 1991, **44**, 3955.
28 Y. Liu, Y. Ding, L. Zhang, P.-X. Gao and Y. Lei, *RSC Adv.*, 2012, **2**, 5193–5198.
29 E. Lemmon, M. McLinden, D. Friend, P. Linstrom and W. Mallard, *NIST Chemistry Webbook, NIST Standard Reference Database Number 69*, National Institute of Standards and Technology, Gaithersburg, MD, 2011, http://www.webbook.nist.gov/chemistry/.
30 J. Lee and S. Han, *Phys. Chem. Chem. Phys.*, 2013, **15**, 18906–18914.
31 M. Bollinger, J. Lauritsen, K. W. Jacobsen, J. K. Nørskov, S. Helveg and F. Besenbacher, *Phys. Rev. Lett.*, 2001, **87**, 196803.
32 Y.-S. Shim, L. Zhang, D. H. Kim, Y. H. Kim, Y. R. Choi, S. H. Nahm, C.-Y. Kang, W. Lee and H. W. Jang, *Sens. Actuators, B*, 2014, **198**, 294–301.
33 E. Comini, *Anal. Chim. Acta*, 2006, **568**, 28–40.
34 V. Dua, S. P. Surwade, S. Ammu, S. R. Agnihotra, S. Jain, K. E. Roberts, S. Park, R. S. Ruoff and S. K. Manohar, *Angew. Chem., Int. Ed.*, 2010, **49**, 2154–2157.
35 J. Li, Y. Lu, Q. Ye, M. Cinke, J. Han and M. Meyyappan, *Nano Lett.*, 2003, **3**, 929–933.